Chinese Physics B

PAPER

# Intrinsic charge transport behaviors in graphene-black phosphorus van der Waals heterojunction devices

To cite this article: Guo-Cai Wang *et al* 2018 *Chinese Phys. B* **27** 077303

View the article online for updates and enhancements.

## Related content

- Direct measurements of conductivity and mobility in millimeter-sized single-crystalline graphene via van der Pauw geometry
  Rui-Song Ma, Qing Huan, Liang-Mei Wu et al.

- From bidirectional rectifier to polarity-controllable transistor in black phosphorus by dual gate modulation
  Guocai Wang, Lihong Bao, Ruisong Ma et al.

- Field-effect transistors based on two-dimensional materials for logic applications
  Wang Xin-Ran, Shi Yi and Zhang Rong

This content was downloaded from IP address 159.226.35.1 on 16/11/2018 at 06:23

Chin. Phys. B Vol. 27, No. 7 (2018) 077303

# Intrinsic charge transport behaviors in graphene-black phosphorus van der Waals heterojunction devices*

Guo-Cai Wang(王国才)[1,2], Liang-Mei Wu(吴良妹)[1,2], Jia-Hao Yan(严佳浩)[1,2], Zhang Zhou(周璋)[1,2], Rui-Song Ma(马瑞松)[1,2], Hai-Fang Yang(杨海方)[1,2], Jun-Jie Li(李俊杰)[1,2], Chang-Zhi Gu(顾长志)[1,2], Li-Hong Bao(鲍丽宏)[1,2,†], Shi-Xuan Du(杜世萱)[1,2], and Hong-Jun Gao(高鸿钧)[1,2]

[1] *Institute of Physics, Chinese Academy of Sciences, Beijing* 100190, *China*
[2] *University of Chinese Academy of Sciences, Beijing* 100190, *China*

(Received 29 March 2018; revised manuscript received 16 April 2018; published online 25 June 2018)

Heterostructures from mechanically-assembled stacks of two-dimensional materials allow for versatile electronic device applications. Here, we demonstrate the intrinsic charge transport behaviors in graphene-black phosphorus heterojunction devices under different charge carrier densities and temperature regimes. At high carrier densities or in the ON state, tunneling through the Schottky barrier at the interface between graphene and black phosphorus dominates at low temperatures. With temperature increasing, the Schottky barrier at the interface is vanishing, and the channel current starts to decrease with increasing temperature, behaving like a metal. While at low carrier densities or in the OFF state, thermal emission over the Schottky barrier at the interface dominates the carriers transport process. A barrier height of $\sim 67.3$ meV can be extracted from the thermal emission-diffusion theory.

**Keywords:** black phosphorus, heterojunction, contact, barrier height

**PACS:** 73.40.Gk, 73.40.Ei, 73.40.Cg, 73.40.Lq **DOI:** 10.1088/1674-1056/27/7/077303

## 1. Introduction

Since the advent of graphene, two-dimensional (2D) materials have generated interest as promising building blocks of next generation ultrathin electronics and optoelectronics.[1–6] Despite the various advantages presented by graphene, the zero-bandgap nature of pristine graphene greatly limits its applications in logic devices due to its high standby power consumption.[3,5,7,8] However, with a finite density of states, the Fermi level of graphene can be readily modified by a gate potential, making graphene an ideal candidate for contact to other 2D materials, which is the basis for fabricating graphene based optoelectronic devices.[9–16] Black phosphorus (BP), as a single elemental (P) layered material, has a thickness-dependent bandgap ranging from 0.3 eV to 1.2 eV with mechanical flexibility,[17–22] high anisotropic charge carrier mobilities,[23–25] and ambient stability via encapsulation or surface decoration,[26–30] all of which make it a promising candidate for applications in future electronics.[23,31–36]

Extensive investigation on BP electronic devices indicates that the device performance, such as the hole mobility and ON state current, is strongly relied on the metal-BP contact.[37] Due to the lack of controllable and sustainable substitutional doping techniques to lower the contact resistance, the common way is to choose contact metals with appropriate work function to inject proper types of carriers into the bands of BP.[38] However, a finite Schottky barrier height is always present at such contacts.[37,38] It is even more challenging when the thickness of BP is smaller than the depletion and transfer lengths since the conventional concepts of the alignment of the Fermi level with the bands of the BP channel break down.[39] Here we investigate the intrinsic transport behaviors in graphene/BP van der Waals heterojunction devices under different carrier densities and temperatures. At high carrier densities ($-40\ \mathrm{V} \le V_{bg} \le 0\ \mathrm{V}$ or $20\ \mathrm{V} \le V_{bg} \le 40\ \mathrm{V}$), tunneling through the Schottky barrier at the graphene/BP dominates at low temperatures. With temperature increasing, the Schottky barrier at the interface is vanishing, and the channel current starts to decrease with increasing temperature, behaving like a metal. On the other hand, at low carrier density or in the OFF state ($V_{bg} = 10$ V), thermal emission over the Schottky barrier at the interface dominates the carriers transport. These results demonstrate that graphene is a good contact electrode for BP devices.

## 2. Experiments

The fabrication process of graphene/BP heterostructures is shown in Fig. 1(a). Firstly, monolayer graphene was grown on Cu foil by the chemical vapor deposition method and then transferred to a 300 nm $SiO_2$/p+ doped Si substrate (I in Fig. 1(a)).[40] After identifying the graphene by optical mi-

*Project supported by the National Basic Research Program of China (Grant No. 2013CBA01600), the National Key Research & Development Project of China (Grant No. 2016YFA0202300), the National Natural Science Foundation of China (Grant Nos. 61474141, 61674170, 61335006, 61390501, 51325204, and 51210003), Youth Innovation Promotion Association of Chinese Academy of Sciences (Grant No. 20150005), and the China Postdoctoral Science Foundation (Grant No. 2017M623146).

†Corresponding author. E-mail: lhbao@iphy.ac.cn

© 2018 Chinese Physical Society and IOP Publishing Ltd 

croscope and Raman spectrum, the sample was transferred into a glove box filled with inert Ar gas. A graphene/BP van der Waals heterojunction was formed by stacking the mechanically exfoliated few-layered BP flakes (∼ 10 nm) onto the graphene flake on the $SiO_2$ substrate (II in Fig. 1(a)). To protect the BP from degradation, a layer of PMMA 495 (A2) was spin coated before taken it out for contact fabrication. An additional thin layer of PMMA 495 (A5) was spin-coated as an electron-beam resist.[41] Reactive ion etching was performed to define the structure of the heterojunction device after electron beam lithography (III in Fig. 1(a)). Finally, a second electron-beam lithography process was employed to define the Ni/Au (5/60 nm) electrical contacts (IV in Fig. 1(a)). To minimize the degradation of BP, all electrical measurements were conducted in a four-probe STM with a vacuum level of $10^{-10}$ mbar. A schematic and a representative optical image of the graphene/BP heterojunction device are shown in Fig. 1(b) and the inset of Fig. 1(c), respectively. The thickness of the BP flake (∼ 10 nm) was determined by atomic force microscopy, as shown in Fig. 1(c). The Raman spectrum of the graphene/BP heterojunction region (marked by a star in Fig. 1(c)) is shown in Fig. 1(d). The observed Raman-active modes of both BP and graphene are consistent with those in previous reports, which demonstrates the high quality of the graphene/BP heterojunction.[42]

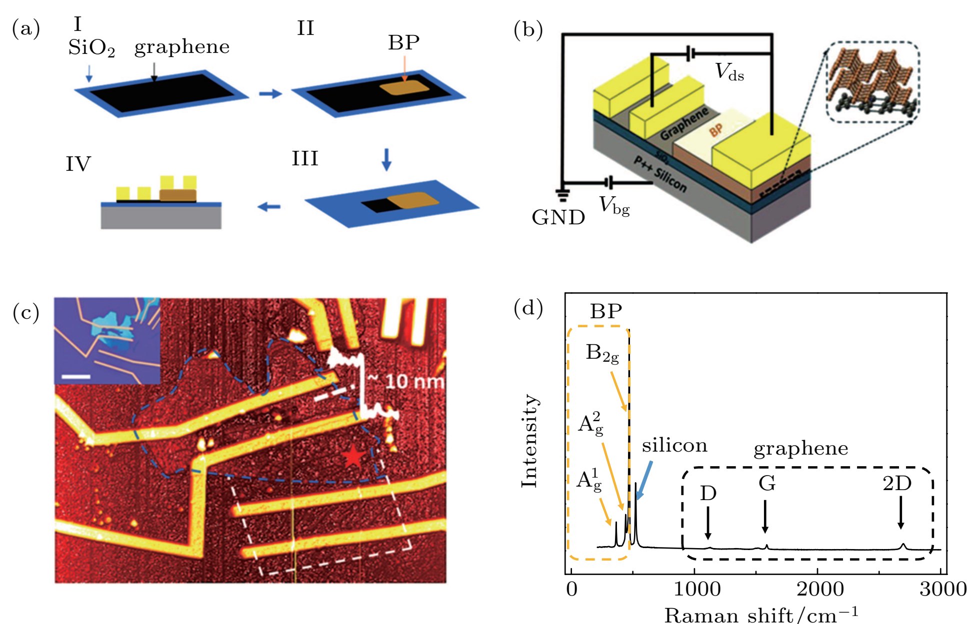


**Fig. 1.** (color online ) (a) Schematic image of the device fabrication process. (b) Schematic image of the graphene/BP heterojunction device. (c) An AFM image of the heterojunction device. Section analysis shows the thickness of the BP flake is ∼ 10 nm. The inset is an optical microscope image of the device (scale bar inset is 10 μm). (d) Raman spectrum collected at the heterojunction region as indicated (red star) in (c).

## 3. Results and discussion

Output characteristics of the graphene device as a function of back gate voltage $V_{bg}$ from −20 V to 20 V at a step of 5 V with source-drain bias voltage $V_{ds}$ from −100 mV to 100 mV are shown in Fig. 2(a). The highly linear behavior at different $V_{bg}$ suggests a good contact between graphene and the Ni/Au electrode. Output characteristics of the pure BP (graphene/BP heterojunction) device are shown in Figs. 2(b) and 2(c) (Figs. 2(d) and 2(e)). A linear behavior can be found for both pure BP (Fig. 2(b)) and graphene/BP heterojunction (Fig. 2(d)) devices at negative gate voltages. A higher drain current delivered in the heterojunction device indicates that graphene is a better contact electrode for holes transport. While for electrons transport (at positive gate voltage bias), apparent non-linearity is observed for the pure BP device (Fig. 2(c)), suggesting that the Schottky barrier is formed at the Ni/BP interface for electron transport. By contrast, the graphene/BP heterojunction device (Fig. 2(e)) delivers a larger drain current and shows a near linear behavior, suggesting that compared to Ni, graphene is also a better contact electrode for electrons transport in BP. This can be further confirmed by the transfer curves shown in Fig. 2(f). Both BP and graphene/BP devices show ambipolar transport behavior, and the graphene/BP heterojunction has enhanced electron transport behavior. The higher drain current in the graphene device ensures that the ambipolar transport in the graphene/BP heterojunction is dominated by the graphene/BP interface rather than the Ni/graphene one. A schematic of the energy band diagram of the heterojunction device at different regimes of $V_{bg}$ is shown in Fig. 2(g). When $V_{bg}$ = 10 V, the Fermi level of graphene is located at the Dirac point and a Schottky barrier forms at the interface between graphene and BP. This Schottky barrier is thinned and lowered when $V_{bg} \gg 10$ V with positive

polarity or $V_{bg} \ll 10$ V with negative polarity due to heavy doping by electrons or holes. It is worth noting that the current minimum occurs at $V_{bg} \sim 20$ V rather than $V_{bg} \sim 10$ V, suggesting that $V_{bg} = 20$ V is the flat band voltage of BP.

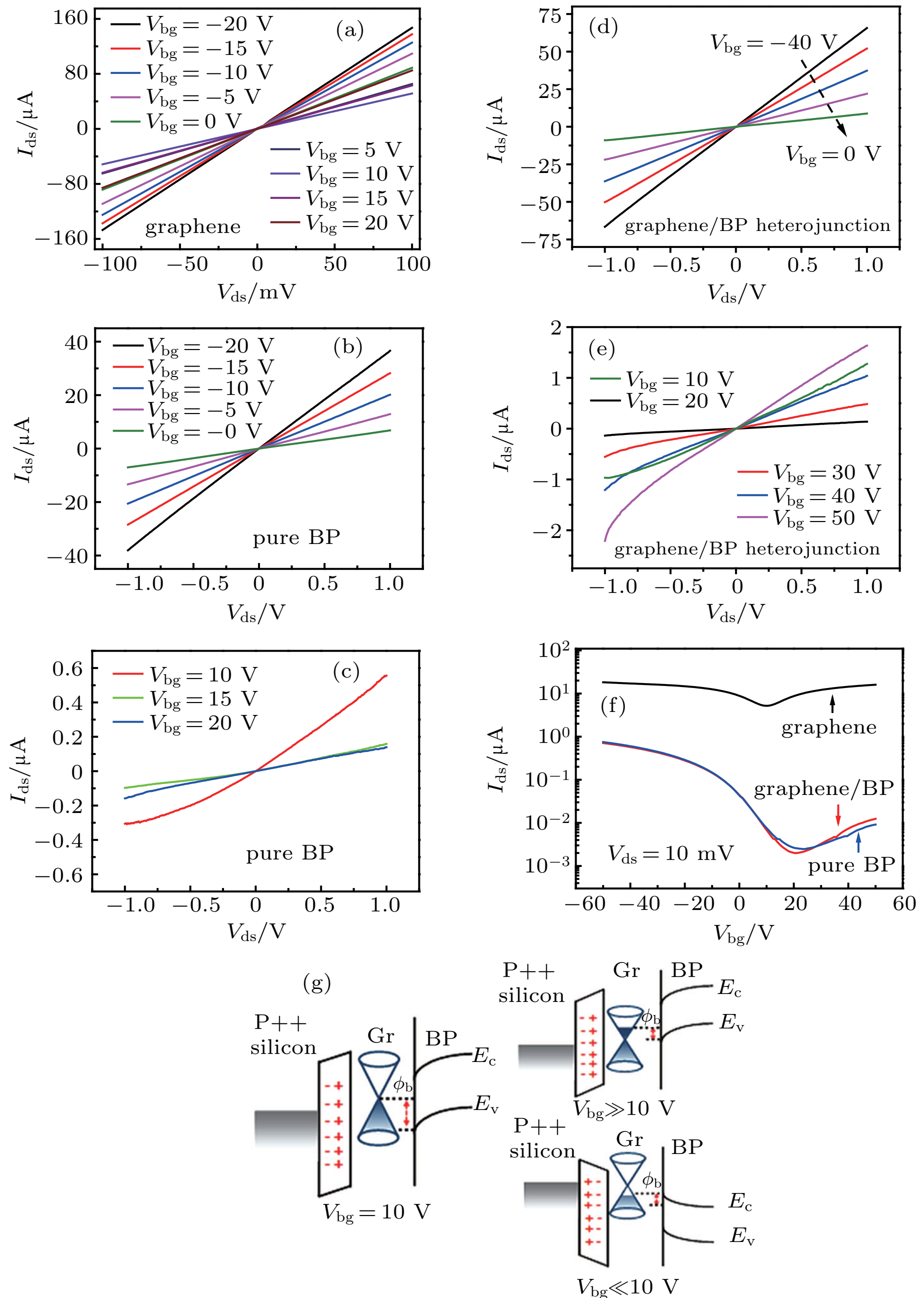

**Fig. 2.** (color online ) (a) Output curves of the graphene device with $V_{ds}$ ranging from −100 mV to 100 mV at different $V_{bg}$ from −50 V to 50 V at a step of 10 V. (b) and (c) Output curves of the BP device with $V_{ds}$ ranging from −1 V to 1 V at $V_{bg}$ from −20 V to 0 V and from 10 V to 20 V at a step of 5 V, respectively. (d) and (e) Output curves of the graphene/BP heterojunction device with $V_{ds}$ ranging from −1 V to 1 V at $V_{bg}$ from −40 V to 0 V and from 10 V to 50 V at a step of 10 V, respectively. (f) Transfer curves of the graphene device (black),the graphene/BP heterojunction device (red), and the BP device (blue) with $V_{ds} = 10$ mV. (g) Schematic of the energy band diagram of the heterojunction device at different $V_{bg}$ regimes.

To probe the intrinsic charge transport behavior in graphene/BP heterojunctions, variable-temperature measurement of the transfer characteristics was performed. Figure 3(a) shows the representative transfer curves of the heterojunction device with temperature increasing from 100 K to 300 K at a step of 20 K. The ON-state current $I_{on}$ ($V_{bg} = -50$ V) shows a weak temperature dependence, while the OFF-state current $I_{off}$ is decreased by nearly three orders of magnitude with decreasing temperature, resulting in a greatly increased on/off current ratio for both holes and electrons. As shown in Fig. 3(b), $I_{on}/I_{off}$ of the device increases with the decreasing temperature; and it increases from 540 to 115000 for holes conduction (black) and from 18.3 to 3700 for electrons conduction (red) when decreasing the temperature from 300 K to 100 K. These results indicate that the thermally activated mechanism dominates the charge transport in the OFF state at

low temperatures.[43] It is found that the gate voltage at which the current reaches its minimum ($V_{\rm off}$) also changes with temperature from $V_{\rm bg} \sim 10$ V at 100 K to $V_{\rm bg} \sim 20$ V at 300 K, as shown in Fig. 3(c), indicating that the charge transport behavior in the heterojunction depends not only on the temperature but also on the charge carrier density. When the temperature is decreased to 100 K, few charge carriers have enough energy to overcome the Schottky barrier at the graphene/BP interface. With the temperature increasing, more charge carriers are thermally excited to overcome the barrier, and $V_{\rm bg}$ corresponding to the current minimum shifts to the flat band voltage of BP.

Based on the metal-semiconductor contact theory,[44] there are two mechanisms for carrier injection from graphene to BP. One is the thermionic emission over the Schottky barrier with an exponential dependence on the temperature, which can be described as

$$I = AA^{*}T^{2}\exp\left(\frac{-q\phi_{\rm b}}{K_{\rm B}T}\right)\left[\exp\left(\frac{qV_{\rm bias}}{\eta K_{\rm B}T}\right)-1\right],$$

where $A$ is the area of the Schottky junction, $A^{*}$ is the effective Richardson constant, $q$ is the elementary charge, $\eta$ is the ideality factor, $K_{\rm B}$ is the Boltzmann constant, and $T$ is the temperature. When the heterojunction device is reversely biased, $\exp\left(\frac{qV_{\rm bias}}{\eta K_{\rm B}T}\right) \ll 1$, the current becomes insensitive to $V_{\rm bias}$ and $I_{\rm sat} \propto AA^{*}T^{2}\exp\left(\frac{-q\phi_{\rm b}}{K_{\rm B}T}\right)$ can be obtained. From the Arrhenius plots of $\ln\,(I_{\rm sat}/T^{2})$ versus $q/K_{\rm B}T$ at different $V_{\rm bg}$ (shown in Figs. 3(d) and 3(e)), the Schottky barrier height $\phi_{\rm b}$ at the graphene/BP interface can be extracted, as shown in Fig. 3(f). At $V_{\rm bg} = 10$ V, a Schottky barrier height of 67.3 meV is obtained. While at other gate voltages, the Schottky barrier is a negative value, suggesting that the thermionic emission model cannot account for the transport behavior at these gate voltages. Therefore, the other mechanism for carrier injection from graphene to BP, the field emission (tunneling) mechanism, is considered,

$$I\,(V,T) = I\,(V,0)\left[1+\frac{(\pi c\,(V)\,K_{\rm B}T)^{2}}{6}\right],$$

where $c(V)$ is a constant related to the tunneling barrier of the junction.[43]

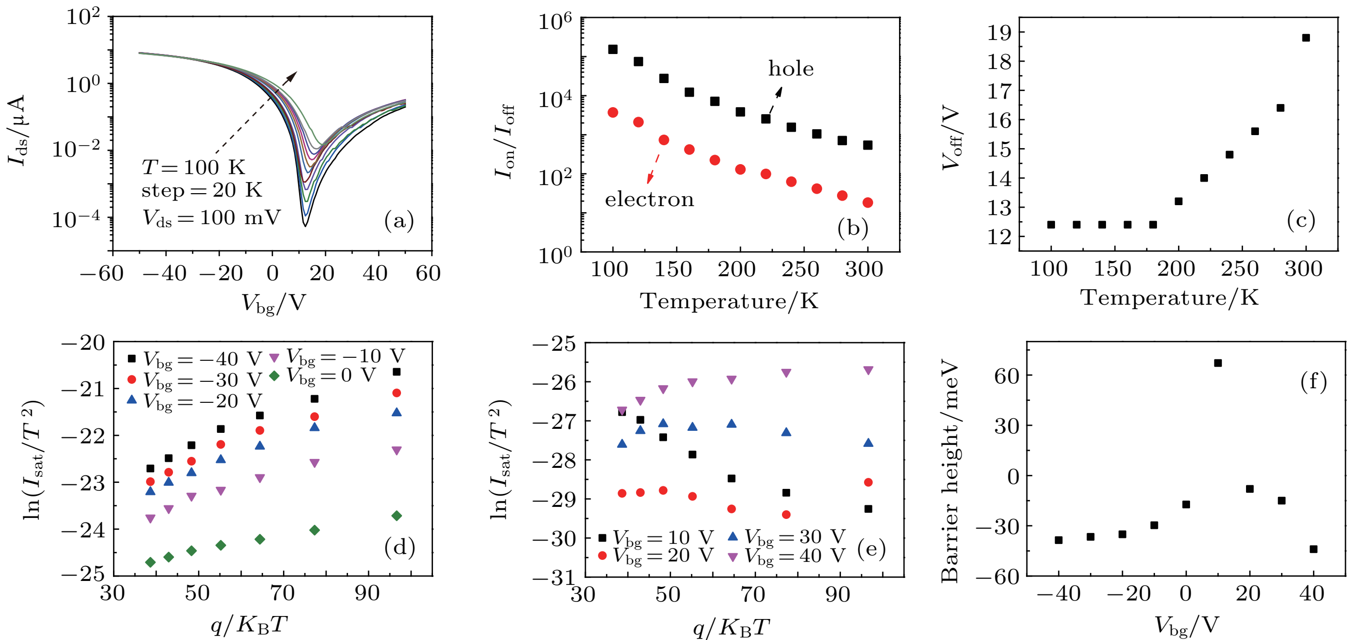


**Fig. 3.** (color online ) (a) Transfer curves of the heterojunction device at different temperatures from 100 K to 300 K at a step of 20 K under a constant bias voltage $V_{\rm ds} = 100$ mV. (b) $I_{\rm on}/I_{\rm off}$ of the heterojunction devices for electrons conduction (red circles) and holes conduction (black squares) at different temperatures. (c) The gate voltages for the OFF states ($V_{\rm off}$) of the heterojunction devices at different temperatures. (d) and (e) Arrhenius plot of $\ln(I_{\rm sat}/T^{2})$ versus $q/K_{\rm B}T$ at different back gate voltages from −40 V to 0 V and from 10 V to 40 V at a step of 10 V, respectively. (f) Extracted Schottky barrier height as a function of the gate voltage.

When the heterojunction device is heavily electron- or hole-doped ($-40\ V \le V_{\rm bg} \le 0$ V or 20 V$\le V_{\rm bg} \le 40$ V), the drain current $I_{\rm ds}$ shows a non-monotonic dependence on the temperature, as shown in the plot of $I_{\rm ds}$ versus $T^{2}$ (Fig. 4(a) for $-40$ V$\le V_{\rm bg} \le 0$ V and Fig. 4(c) for 20 V$\le V_{\rm bg} \le 40$ V). At low temperatures, $I_{\rm ds}$ increases with the increasing temperature and linear fitting of the $I_{\rm ds}$ curves as a function of $T^{2}$ at different gate voltages can determine the temperature $T_{\rm Tunnel}$ below which tunneling transport dominates, as shown in Figs. 4(a) and 4(c). Figures 4(b) and 4(d) show $T_{\rm Tunnel}$ as a function of the gate voltage. $T_{\rm Tunnel}$ decreases with increasing carrier densities (holes or electrons), implying that the height or the width of the Schottky barrier decreases with increasing charge carrier densities. At higher temperatures, on the other hand, $I_{\rm ds}$ decreases with the increasing temperature, behaving like a metal.[45]

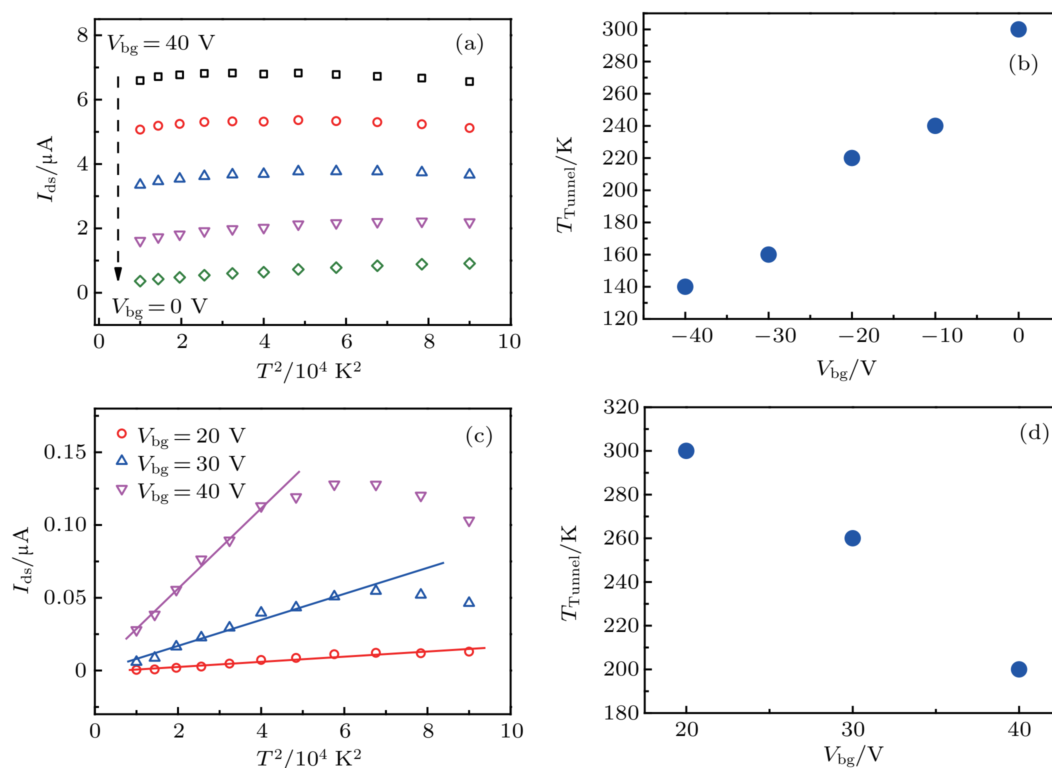


**Fig. 4.** (color online ) (a) Plots of $I_{ds}$ as a function of $T^2$ at different $V_{bg}$ from −40 V to 0 V at a step of 10 V. (b) Plots of $T_{Tunnel}$ as a function of $V_{bg}$. (c) Plots of $I_{ds}$ as a function of $T^2$ at $V_{bg}$ from 20 V to 40 V at a step of 10 V. (d) Plots of $T_{Tunnel}$ as a function of $V_{bg}$.

## 4. Conclusion

We have investigated the intrinsic charge transport behavior in the graphene/BP heterojunction. It is found that the transport behaviors of the heterojunction devices depend on the carrier density and temperature. At high carrier densities, tunneling through the Schottky barrier at the graphene/black phosphorus dominates at low temperatures. With temperature increasing, the Schottky barrier at the interface is vanishing, and the channel current starts to decrease with increasing temperature, behaving like a metal. Finally, at low carrier density or in the OFF state, thermal emission over the Schottky barrier at the interface dominates the carrier transport.


## Acknowledgment

The authors would like to thank Prof. Sokrates Pantelides for the valuable discussion.


## References


[1] Geim A K and Novoselov K S 2007 *Nat. Mater.* **6** 183
[2] Novoselov K S, Jiang D, Schedin F, Booth T J, Khotkevich V V, Morozov S V and Geim A K 2005 *Proc. Natl. Acad. Sci. USA* **102** 10451
[3] Schwierz F 2010 *Nat. Nanotechnol.* **5** 487
[4] Radisavljevic B, Radenovic A, Brivio J, Giacometti V and Kis A 2011 *Nat. Nanotechnol.* **6** 147
[5] Fiori G, Bonaccorso F, Iannaccone G, Palacios T, Neumaier D, Seabaugh A, Banerjee S K and Colombo L 2014 *Nat. Nanotechnol.* **9** 768
[6] Guo H, Lu H L, Huang L, Wang X Y, Lin X, Wang Y L, Du S X and Gao H J 2017 *Acta Phys. Sin.* **66** 216803 (in Chinese)
[7] Castro Neto A H, Guinea F, Peres N M R, Novoselov K S and Geim A K 2009 *Rev. Mod. Phys.* **81** 109
[8] Butler S Z, Hollen S M, Cao L, Cui Y, Gupta J A, Gutiérrez H R, Heinz F, Hong S S, Huang J and Ismach A F 2013 *ACS Nano* **7** 2898
[9] Liu Y, Wu H, Cheng H C, Yang S, Zhu E B, He Q Y, Ding M N, Li D H, Guo J, Weiss N O, Huang Y and Duan X F 2015 *Nano Lett.* **15** 3030
[10] Shim J and Park J H 2016 *Org. Electron.* **33** 172
[11] Roy K, Padmanabhan M, Goswami S, Sai T P, Ramalingam G, Raghavan S and Ghosh A 2013 *Nat. Nanotechnol.* **8** 826
[12] Meng J, Song H D, Li C Z, Jin Y, Tang L, Liu D, Liao Z M, Xiu F and Yu D P 2015 *Nanoscale* **7** 11611
[13] Su W J, Chang H C, Shih Y T, Wang Y P, Hsu H P, Huang Y S and Lee K Y 2016 *J. Alloys Compd.* **671** 276
[14] Moriya R, Yamaguchi T, Inoue Y, Morikawa S, Sata Y, Masubuchi S and Machida T 2014 *Appl. Phys. Lett.* **105** 083119
[15] Yoon J, Park W, Bae G Y, Kim Y, Jang H S, Hyun Y, Lim S K, Kahng Y H, Hong W K and Lee B H 2013 *Small* **9** 3295
[16] Das S, Gulotty R, Sumant A V and Roelofs A 2014 *Nano Lett.* **14** 2861
[17] Guan J, Zhu Z and Tomanek D 2014 *ACS Nano* **8** 12763
[18] Zhu W, Yogeesh M N, Yang S, Aldave S H, Kim J S, Sonde S, Tao L, Lu N and Akinwande D 2015 *Nano Lett.* **15** 1883
[19] Jiang J W and Park H S 2014 *J. Phys. D: Appl. Phys.* **47** 385304
[20] Das S, Zhang W, Demarteau M, Hoffmann A, Dubey M and Roelofs A 2014 *Nano Lett.* **14** 5733
[21] Pan D X, Wang T C and Guo W L 2015 *Chin. Phys. B* **24** 86401
[22] Yan S L, Xie Z J, Chen J H, Taniguchi T and Watanabe K J 2017 *Chin. Phys. Lett.* **34** 047304
[23] Qiao J S, Kong X, Hu Z X, Yang F and Ji W 2014 *Nat. Commun.* **5** 4475
[24] Baba M, Nakamura Y, Takeda Y, Shibata K, Morita A, Koike Y and Fukase T 1992 *J. Phys.: Condens. Matter* **4** 1535
[25] Wang H, Wang X M, Xia F N, Wang L H, Jiang H, Xia Q F, Chin M L, Dubey M and Han S J 2014 *Nano Lett.* **14** 6424
[26] Cao Y, Mishchenko A, Yu G L, Khestanova E, Rooney A P, Prestat E, Kretinin A V, Blake P, Shalom M B, Woods C, Chapman J, Balakrishnan G, Grigorieva I V, Novoselov K S, Piot B A, Potemski M, Watanabe K, Taniguchi T, Haigh S J, Geim A K and Gorbachev R V 2015 *Nano Lett.* **15** 4914
[27] Liu H, Neal A T, Si M W, Du Y C and Ye P D 2014 *IEEE Electron. Device Lett.* **35** 795

[28] Luo X, Rahbarihagh Y, Hwang J C M, Liu H, Du Y C and Ye P D 2014 *IEEE Electron. Device Lett.* **35** 1314
[29] Avsar A, Vera-Marun I J, Tan J Y, Watanabe K, Taniguchi T, Castro Neto A H and Ozyilmaz B 2015 *ACS Nano* **9** 4138
[30] Qiao J S, L Z and Ji W 2017 *Chin. Phys. B* **26** 36803
[31] Castellanos-Gomez A 2015 *J. Phys. Chem. Lett.* **6** 4280
[32] Gillgren N, Wickramaratne D, Shi Y M, Espiritu T, Yang J W, Hu J, Wei J, Liu X, Mao Z Q, Watanabe K, Taniguchi T, Bockrath M, Barlas Y, Lake R K and Lau C N 2015 *2D Mater.* **2** 011001
[33] Liu H, Neal A T, Zhu Z, Luo Z, Xu X, Tomanek D and Ye P D 2014 *ACS Nano* **8** 4033
[34] Koenig S P, Doganov R A, Schmidt H, Castro Neto A H and Zyilmaz B 2014 *Appl. Phys. Lett.* **104** 103106
[35] Xia F, Wang H and Jia Y 2014 *Nat. Commun.* **5** 4458
[36] Li X F, Xiong X and Wu Y Q 2017 *Chin. Phys. B* **26** 37307
[37] Du Y C, Liu H, Deng Y X and Ye P D 2014 *ACS Nano* **8** 10035
[38] Das S, Demarteau M and Roelofs A 2014 *ACS Nano* **8** 11730
[39] Allain A, Kang J, Banerjee K and Kis A 2015 *Nat. Mater.* **14** 1195
[40] Guo W, Jing F, Xiao J, Zhou C, Lin Y W and Wang S 2016 *Adv. Mater.* **28** 3152
[41] Wang G C, Bao L H, Pei T F, Ma R S, Zhang Y Y, Sun L L, Zhang G Y, Yang H F, Li J J, Gu C Z, Du S X, Pantelides S T, Schrimpf R D and Gao H J 2016 *Nano Lett.* **16** 6870
[42] Li L K, Yu Y J, Ye G J, Ge Q Q, Ou X D, Wu H, Feng D L, Chen X H and Zhang Y B 2014 *Nat. Nanotechnol.* **9** 372
[43] Kang J, Jariwala D, Ryder C R, Wells S A, Choi Y, Hwang E, Cho J H, Marks T J and Hersam M C 2016 *Nano Lett.* **16** 2580
[44] Sze S M and Ng K K 2006 *Physics of Semiconductor Devices* (New York: John Wiley & Sons) p. 134
[45] Saito Y and Iwasa Y 2015 *ACS Nano* **9** 3192